Adsorption (2012) 18:199–211
DOI 10.1007/s10450-012-9394-2

Effect of CO_2 activation of carbon xerogels on the adsorption of methylene blue

Carlos A. Páez · María S. Contreras · Angélique Léonard · Silvia Blacher · Claudio G. Olivera-Fuentes · Jean-Paul Pirard · Nathalie Job

Received: 16 September 2011 / Accepted: 8 June 2012 / Published online: 28 June 2012

Abstract The effect of physical activation with CO_2 of carbon xerogels, synthesized by pyrolysis of a resorcinol-formaldehyde aqueous gel, on the adsorption capacities of Methylene Blue (MB) was studied. The activation with CO_2 lead to carbon materials with micropore volumes ranging from 0.28 to 0.98 $cm^3\,g_C^{-1}$. MB-adsorption isotherm studies showed that the increase of micropore volume and corresponding surface area led to: (i) a significant improvement in the capacity of MB-adsorption at monolayer coverage, from 212 to 714 $mg\,g_C^{-1}$, and (ii) an increase of the binding energy related to Langmuir isotherm constant up to 45 times greater than those of commercial microporous activated carbons used as reference (NORIT R2030, CALGON BPL and CALGON NC35). It is proposed that the increase of the binding energy results from chemical cleaning of the O-groups onto carbon surface as a consequence of CO_2-activation, increasing the π–π interaction between MB and graphene layers of the carbon xerogels. Finally, a series of batch kinetics were performed to investigate the effect of CO_2-activation conditions on the mechanism of MB-adsorption. Experimental data were fitted using pseudo-first-order, pseudo-second-order and intraparticle diffusion kinetic models. From pseudo-second-order kinetic model, one observes an increase in the initial rate of MB-adsorption from 0.019 to 0.0565 min^{-1}, by increasing the specific surface area from 630 to 2180 $m^2\,g_C^{-1}$ *via* CO_2-activation. Depending on the activation degree of the carbons, two different mechanisms control the MB-adsorption rate: (i) at low activation degree, the intraparticle diffusion is the rate-limiting phenomenon, whereas (ii) at high activation degree, the reactions occurring at the solid/liquid interface are the rate-limiting steps.

Keywords Carbon xerogel · CO_2-activation · Methylene blue adsorption · Kinetics · Intraparticle diffusion

1 Introduction

In the world, around two hundred tons of dyes are discharged in effluents annually, causing serious environmental problems (Jin et al. 2007). Even at very low concentration, these dyes affect the nature of the water: they inhibit sunlight penetration, they reduce photosynthetic action and some of the dyes are carcinogenic and mutagenic (Nacèra and Aicha 2006; Yu et al. 2009). In the search of solutions for these environmental problems, different physicochemical technologies have been proposed: adsorption (Rafatullah et al. 2010), coagulation (Stephenson and Duff 1996), flocculation (Szygula et al. 2009), precipitation (Stephenson and Duff 1996), photo-catalytic degradation (Páez et al. 2010; Granados O et al. 2005), biodegradation (Elisangela et al. 2009), ion-exchange (Labanda et al. 2011), reverse osmosis and ultra-filtration (Nataraj et al. 2009). Of all, the adsorption process has been found to be superior to other technologies in terms of initial costs, simplicity of design, operation and insensitivity to toxic substrates (Karaca et al. 2008). Specially, activated carbons (ACs) are adsorbents the most widely used with great success because of their high adsorption capacity (Hamdaoui 2006). This

C.A. Páez (✉) · M.S. Contreras · A. Léonard · S. Blacher · J.-P. Pirard · N. Job
Laboratory of Chemical Engineering, Department of Applied Chemistry, University of Liège, B6a, 4000 Liège, Belgium
e-mail: cpaez@ulg.ac.be

M.S. Contreras · C.G. Olivera-Fuentes
TADiP Group, Department of Thermodynamics and Transport Phenomena, Simón Bolívar University, Caracas 1080, Venezuela

adsorption capacity has been demonstrated in the adsorption of dyes such as Malachite Green (MG), Rhodamine B (RB), Reactive Black 5 (RB5) and Methylene Blue (MB), reaching dye-adsorption capacities from aqueous solutions up to 480, 556, 280 and 435 mg of dye per g of activated carbon, respectively (Yu et al. 2009; Ip et al. 2010; Wang et al. 2010).

Specifically, Methylene Blue (MB) is a colorant that can be found in textile fibers like cotton, wood or silk; its adsorption from aqueous solutions is a useful tool for product control of adsorbents (Rafatullah et al. 2010; Hamdaoui 2006). In fact, numerous equilibrium, kinetic and thermodynamic studies (Rafatullah et al. 2010; Kannan and Sundaram 2001; El Qada et al. 2008; Raposo et al. 2009; Stavropoulos and Zabaniotou 2005; Tan et al. 2008; Yamashita et al. 2001) use MB as model adsorbent to compare the performance of various ACs prepared from very different sources. Some of these studies show that the total adsorption capacity of activated carbons is directly linked to the specific surface area, the specific pore volume and the pore size distribution of the adsorbent (Stavropoulos and Zabaniotou 2005; Tan et al. 2008; Yamashita et al. 2001). However, active carbons issued from natural sources are often mainly microporous, with low meso- or macropore volume, which may induce diffusional limitations in dynamic processes like adsorption or catalysis. Increasing the volume of large pores while keeping high specific surface areas should minimize the diffusional limitations inside carbons without damaging their adsorption capacity (Contreras et al. 2010; Job et al. 2006). In this context, porous carbon materials with high specific surface area and large meso- and macropore volume with well-controlled size are interesting, and researches turn towards synthetic nano- or mesostructured materials with well-controlled pore texture.

Among these new materials, carbon xerogels (CXs) have proved to be excellent alternatives to activated carbons in various processes (Contreras et al. 2010; Job et al. 2006, 2004; Zubizarreta et al. 2008, 2009; Gommes et al. 2008). These materials, prepared by polycondensation of a phenol (commonly, resorcinol) and formaldehyde in a solvent (water in most cases) are composed of microporous interconnected sphere-like nodules, formed during the gel synthesis *via* a microphase separation mechanism induced by polymer growth (Gommes et al. 2008). The size of these nodules is mainly regulated by the synthesis pH (Job et al. 2004); as a result, the size of the voids between the nodules after drying and pyrolysis, and thus the meso- or macroporosity of the final carbon material, is also regulated: it depends on both the composition of the precursor solution (pH, mainly) and the drying procedure (Job et al. 2004). For specific applications, and despite their higher cost, carbon xerogels are interesting: the accurate tailoring of the pore texture leads to increasing significantly the performance of catalytic and electrocatalytic processes and could be applied to dynamic adsorption. For example, Girgis et al. (2011) studied the MB-adsorption capacity of a series of CXs synthesized from resorcinol-formaldehyde resins pyrolyzed at a temperature ranging from 500 to 700 °C. The results showed a good MB-adsorption capacity (222 mg g_C^{-1}) for the carbon xerogel pyrolyzed at 700 °C, which displayed a specific surface area of 735 $m^2\,g_C^{-1}$. However, to increase the adsorption capacity, the relatively low inner surface ($\sim$ 700 $m^2\,g_C^{-1}$) of CXs must be developed, for example by chemical or physical activation.

In a recent study, Contreras et al. (2010) carried out the physical activation of highly mesoporous CXs with CO_2 and studied the influence of activation temperature and activation time on their final physicochemical properties. It was found that this process produces an increase of the micropore volume and of the specific surface area without altering the meso-macroporosity developed during the xerogel synthesis. In addition, the specific surface area increases quite linearly with the burn-off degree, from $\sim$ 600 $m^2\,g_C^{-1}$ to around 2000 $m^2\,g_C^{-1}$. Thus, it is possible to control the surface development easily. Finally, the material obtained is extremely clean, with low ash and oxygen surface group content. All these results offer an excellent basis for the use of CO_2-activated carbon xerogels in water decontamination, specifically in dynamic dye-adsorption processes.

In the present study, a carbon xerogel with large mesopores (mesopore size ranging from 28 to 40 nm, pore volume of 1.3 $cm^3\,g_C^{-1}$) was synthesized and physically activated with CO_2 under various conditions. The resulting materials, with specific surface areas ranging from 630 $m^2\,g_C^{-1}$ to 2180 $m^2\,g_C^{-1}$, were used as adsorbents to remove Methylene Blue (MB) from aqueous solutions. In order to investigate the influence of the surface development on the MB-absorption capacities of these carbon xerogels, equilibrium isotherms were measured and kinetics studies were performed. Langmuir and Freundlich models (Ip et al. 2010; Allen et al. 2004; Langmuir 1918; Freundlich 1906; Misra 1969) were used to fit the adsorption equilibrium data, whereas adsorption kinetics data were analyzed through pseudo-first-order, pseudo-second-order and intraparticle diffusion models (Ip et al. 2010; Wang et al. 2010). Finally, the capacity and kinetics of MB adsorption of the activated carbon xerogels were compared to those of common commercial activated carbons (NORIT R2030, CALGON BPL and CALGON NC35).

2 Experimental

2.1 Selection of carbon xerogels

The activated carbon xerogels used in the present study are the same as those prepared by Contreras et al. (2010)

in a previous work. To summarize, one organic aqueous gel was synthesized by polycondensation of resorcinol with formaldehyde in water, using sodium carbonate as basification agent. The resorcinol/formaldehyde molar ratio, R/F, was fixed at 0.5; the resorcinol/sodium carbonate molar ratio, R/C, was chosen equal to 1000; the dilution ratio, D, *i.e.* the water/reactant molar ratio, was equal to 5.7. 160.0 g resorcinol (Vel, 99 %) and 0.1540 g sodium carbonate were first mixed with 303.5 mL deionized water. Then, 263.1 mL of formaldehyde solution (Aldrich, 37 wt.% in water; stabilized by 10–15 wt.% methanol) were added. Gelation and aging were then performed at 70 °C in an oven during 72 h in sealed flasks. Organic xerogels were obtained by vacuum drying without any sample pre-treatment, *i.e.* without solvent exchange prior to drying. The unsealed flasks were simply kept at 60 °C and the pressure was progressively decreased in two days from 10^5 Pa to 10^3 Pa. The samples were then heated to 150 °C at 10^3 Pa during 12 h. The resulting xerogel was pyrolyzed at 900 °C in 4.1×10^{-3} mol min^{-1} flowing nitrogen and was sifted to obtain 50–100 µm diameter particles; this sample is labeled as CX.

From CX, three activated carbon xerogels were obtained by physical activation with pure flowing CO_2 (4.1×10^{-3} mol min^{-1}) at 900 °C for 4, 8 and 16 h. The samples are labelled as follows: the letters CX (for 'carbon xerogel' are followed by the activation temperature (900 °C) and the activation duration (4, 8 or 16 h). For example, the sample CX-900-8 was obtained by activation of CX at 900 °C for 8 h. Finally, three commercial microporous activated carbons were selected for comparison: NORIT R2030, CALGON BPL and CALGON NC35, designed in the following paragraphs as R2030, BPL and NC35, respectively. Note that microporous commercial materials were selected as reference to better highlight the effect of the presence of mesoporosity on the micropore access in the case of activated carbon xerogels.

2.2 Physical and chemical characterization of carbon xerogels

The pore texture of all carbons was determined by analysis of the N_2 adsorption-desorption isotherms, performed at −196 °C with a Sorptomatic Carlo Erba 1900. The analysis of the isotherms provided the specific surface area, S_{BET}, the specific micropore volume, V_{DUB-N_2} and the total pore volume, V_V. The minimum and maximum mesopore diameters, $d_{p,min}$ and $d_{p,max}$, *i.e.* the limit under which smaller pores represent 5 % and 95 % of the mesopore volume, respectively, were determined from mesopore size distribution calculated by the Broekhoff-de-Boer method using the adsorption branch of the isotherm. The methods for analysis of the isotherms are described in Contreras et al. (2010). Temperature-Programmed-Desorption (TPD) of CO and CO_2, which gives access to the surface chemistry of the samples (Figueiredo et al. 1999), were carried out with an automatic analyzer Micromeritics AutoChem II monitoring the amount of desorbed CO, n_{CO}, and CO_2, n_{CO_2}, with an Omnistar Pfeiffer mass spectrometer. Finally, the pH value to which the electrical charge density on the carbon surfaces is zero (point of zero charge, PZC) was determined by the method of Park and Regalbuto (Contreras et al. 2010; Regalbuto 2007; Lambert et al. 2009). Data concerning the carbon xerogels presented below are those obtained by Contreras et al. (2010) in a previous work. The carbons R2030, BPL and NC35 were analyzed in the ambit of the present study.

2.3 Adsorption equilibrium isotherms

The present section describes the adsorption of Methylene Blue (MB) from water solutions at 20 °C and with a constant pH close to 6.5. This test is commonly used for tracer studies on activated carbons (Potgieter 1991). A MB-solution with a concentration of 6 mg L^{-1} was prepared from analytical-grade reagent (Sigma-Aldrich, $Cl_6H_{18}ClN_3S{\cdot}3H_2O$, dye content >82 %) and distilled water. Adsorption isotherms were obtained as follows: accurately weighed amounts, from 4 to 30 mg, of adsorbent were placed in ten separate 25 mL flasks, each containing 20 mL of the 6 mg L^{-1} MB aqueous solution. The flasks were then stopped, placed into a thermostatic bath and continuously stirred for 72 h to reach equilibrium. All the experimental runs were conducted at 20 °C. The concentration of MB in each flask, before and after adsorption equilibrium, was measured using a UV-visible spectrophotometer MILTON ROY 401, at a wavelength of 665 nm.

2.4 Kinetics of adsorption

Batch adsorption kinetic experiments were carried out by stirring 0.5 g of activated carbon (pellets diameter range of 50–100 µm) at 100 rpm in 500 mL of MB aqueous solution (3.7 mg L^{-1}) in a glass flask placed in a thermostatic bath at a constant temperature of 20 °C and at a constant pH of 6.5. The glass flask was equipped with an immersion probe of 10 mm path length for the monitoring of MB concentration. This probe was protected with a metallic sieve of 45 µm. The MB solution was analyzed every 5 min using a visible spectrophotometer, Metrohm 662, at a wavelength of 665 nm.

3 Results

3.1 Textural properties

For all the carbons, the values of specific surface area, S_{BET}, specific micropore volume, V_{DUB-N_2}, total pore volume,

V_V, and minimum and maximum pore diameters, $d_{p,min}$ and $d_{p,max}$, are displayed in Table 1. These results are those obtained in a previous work (see Table 1 in Contreras et al. 2010). As concluded by Contreras et al. (2010), the micropores develop with both the activation temperature, T_{act}, and the activation time, t_{act} : S_{BET}, V_{DUB-N_2} and V_V undergo a significant increase when T_{act} and/or t_{act} increase(s). In particular S_{BET}, which is 630 $m^2\,g_C^{-1}$ for CX increases to 1015, 1365 and 2180 $m^2\,g_C^{-1}$ for CX-900-4, CX-900-8 and CX-900-16, respectively. In parallel, V_{DUB-N_2} increases from 0.28 (CX) to 0.98 $cm^3\,g_C^{-1}$ (CX-900-16) and V_V from 1.3 (CX) to 2.8 $cm^3\,g_C^{-1}$ (CX-900-16). However, the activation with CO_2 does not modify the mesopore size, which ranges from 28 nm ($d_{p,min}$) to 40 nm, ($d_{p,max}$). Comparatively, commercial activated carbons showed S_{BET} values between 824 and 1185 $m^2\,g_C^{-1}$, V_{DUB-N_2} values from 0.34 to 0.48 $cm^3\,g_C^{-1}$ and pore volume values, V_V, of 0.6, 0.7 and 2.7 $cm^3\,g_C^{-1}$ for NC35, BPL and R2030, respectively (Table 1).

Table 1 Pore texture characterization obtained by N_2-sorption

Sample	N_2 adsorption				
	S_{BET} ($m^2\,g_C^{-1}$)[a] ±10	V_{DUB-N_2} ($m^3\,g_C^{-1}$)[a] ±0.01	V_V ($m^3\,g_C^{-1}$)[a] ±0.1	$d_{p,min}$ (nm) ±2	$d_{p,max}$ (nm) ±2
CX	630	0.28	1.3	28	40
CX-900-4	1015	0.42	1.7	29	40
CX-900-8	1365	0.57	2.0	28	43
CX-900-16	2180	0.98	2.8	29	41
R2030	897	0.35	2.7	–[b]	–[b]
NC35	1185	0.48	0.6	–[b]	–[b]
BPL	824	0.34	0.7	–[b]	–[b]

S_{BET}: specific surface area calculated by BET equation; V_{DUB-N_2}: micropore volume determined from nitrogen adsorption by the Dubinin-Radushkevich equation; V_V: total pore volume determined from nitrogen adsorption at saturation; $d_{p,min}$ and $d_{p,max}$: minimum and maximum mesopore diameters.

Note: For the CX series, the values of S_{BET}, V_{DUB-N_2}, V_V, $d_{p,min}$ and $d_{p,max}$ were obtained from Contreras et al. (2010)

[a] g_C corresponds to gram of carbon

[b] Not pertinent, the pore size distribution being outstretched from micropores to µm-sized pores

3.2 Surface chemistry characterization

The values of PZC for commercial and synthesized carbons are shown in Table 2. In the case of the CX series, the differences between PZC values are not significant despite the activation treatment: the pH at which the carbon surface has a net neutral charge is in the 8.2–8.6 range. TPD spectra of carbons xerogels before and after activation are discussed in depth elsewhere (Contreras et al. 2010). Table 2 summarizes the quantities of CO and CO_2 desorbed, n_{CO} and n_{CO_2} of all carbons. Table 2 also reports the amount of CO or CO_2 desorbed per specific surface area unit, $n_{A,CO}$ and n_{A,CO_2}. The non-activated carbon xerogel, CX, and the commercial carbons displayed higher $n_{A,CO}$ and n_{A,CO_2} values, in the 0.67–1.14 µmol $g_C^{-1}\,m^{-2}$ range for $n_{A,CO}$ and from 0.23 to 0.44 µmol $g_C^{-1}\,m^{-2}$ for n_{A,CO_2}. Figure 1b shows the evolution of the $n_{A,CO}$ and n_{A,CO_2} with the increase of the specific surface area, S_{BET}, for the non-activated and activated carbon xerogels. Although the nature of the oxygen surface groups does not change drastically with the activation conditions (Contreras et al. 2010), the amount calculated of CO (or CO_2) desorbed by surface area unit decreases considerably with the increase of S_{BET}: from 0.79 to 0.19 µmol $g_C^{-1}\,m^{-2}$ for $n_{A,CO}$ and from 0.23 to 0.056 µmol $g_C^{-1}\,m^{-2}$ for n_{A,CO_2} (Fig. 1b).

3.3 Adsorption equilibrium isotherms

From experimental data and in order to determine the amount (mg) of MB adsorbed (mg_{MB}) by gram of the carbon used (g_C), q_e ($mg_{MB}\,g_C^{-1}$), the following equation was used:

$$q_e = \frac{(C_0 - C_e)V}{W} \quad (1)$$

Table 2 Surface characterization

Sample	PZC ±0.05	n_{CO} (µmol g_C^{-1})[a] ±20	n_{CO_2} (µmol g_C^{-1})[a] ±20	$n_{A,CO}$ (µmol $g_C^{-1}\,m^{-2}$)[a] ±0.02	n_{A,CO_2} (µmol $g_C^{-1}\,m^{-2}$)[a] ±0.02
CX	8.2	500	148	0.79	0.23
CX-900-4	8.6	457	114	0.45	0.11
CX-900-8	8.6	405	133	0.29	0.09
CX-900-16	8.6	427	123	0.19	0.05
R2030	10.0	606	296	0.67	0.33
NC35	9.4	1139	522	0.96	0.44
BPL	7.6	945	216	1.14	0.26

[a] g_C correspond to gram of carbon

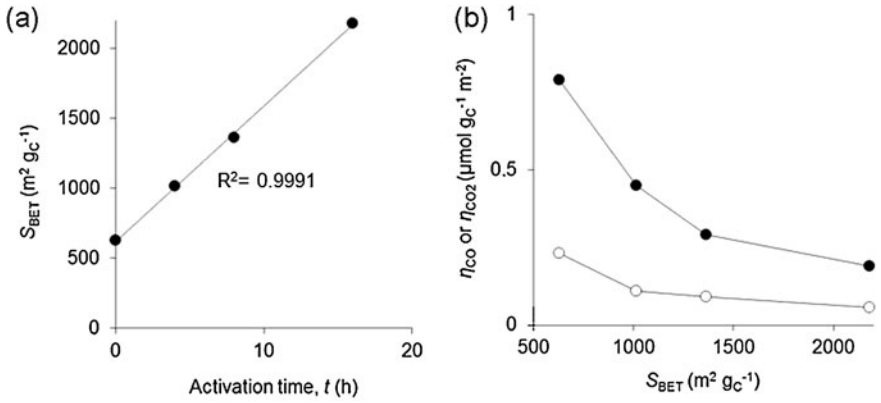

Fig. 1 (**a**) Specific surface area, S_{BET}, for carbon xerogels activated at 900 °C as a function of the activation time: (**b**) amount of desorbed CO (•) and CO_2 (○) per specific surface area unit as a function of the specific surface area, S_{BET}

where C_0 and C_e are the initial and equilibrium liquid-phase concentrations of MB (mg_{MB} L^{-1}), respectively, V is the volume of the MB solution (L) and W is the mass of carbon used (g_C). In this study, the equilibrium data were analyzed using both the Langmuir model and the Freundlich model (Eqs. (2) and (3), respectively) (Ip et al. 2010; Allen et al. 2004; Langmuir 1918; Freundlich 1906; Misra 1969):

$$q_e = \frac{k_L q_{max} C_e}{1 + k_L C_e} \tag{2}$$

$$q_e = k_F C_e^{1/n} \tag{3}$$

where q_{max} is the monolayer capacity of the adsorbent ($mg_{MB}\, g_C^{-1}$), k_L is the Langmuir adsorption constant ($L\, g_C^{-1}$), k_F ($mg_{MB}^{1-(1/n)}\, L^{1/n}\, g_C^{-1}$) and n are the Freundlich constants.

For convenience of analysis, both equations can be rearranged into a linear form. So, on the one hand, the analysis of the experimental adsorption data of MB was performed by applying the linear Langmuir model equation (4):

$$q_e = \frac{1}{q_{max} k_L} \times \frac{1}{C_e} + \frac{1}{q_{max}} \tag{4}$$

In this case, the plot of $1/q_e$ against $1/C_e$ should be linear with a slope of $1/(q_{max} k_L)$ and an intercept of $1/q_{max}$ on the $1/q_e$ axis. On the other hand, the Freundlich model becomes:

$$\ln q_e = \ln k_F + \frac{1}{n} \times \ln C_e \tag{5}$$

In this case, a graph of $\ln q_e$ against $\ln C_e$ should be linear with a slope of $1/n$ and an intercept of $\ln k_F$ on the $\ln q_e$ axis. The data obtained for all the carbons are well fitted by the linearized form of the Langmuir (Eq. (4)) or Freundlich (Eq. (5)) isotherms over the whole MB-concentration range used, with correlation coefficient values $R^2 > 0.990$. Afterwards, the isotherm constants were, in both cases, determined by minimizing the difference between experimental and theoretical data using the normalized percentage of deviation, P (%), calculated by:

$$P(\%) = \frac{100}{N} \times \sum_{i=1}^{N} \left| \frac{q_{e,cal} - q_e}{q_e} \right|_i \tag{6}$$

where N is the number of experimental data points and $q_{e,cal}$ is the theoretical amount of MB adsorbed at equilibrium. Table 3 displays the values of q_{max}, k_L, n and k_F of all adsorbents after minimization process. Figure 2 compares the experimental data of the synthesized carbon xerogels activated at 900 °C (Figs. 2a–2b) with those of the commercial activated carbons (Figs. 2c–2d) using both the Langmuir and Freundlich isotherm models. In addition, Figs. 3a–3d display the behavior of Langmuir and Freundlich parameters, q_{max}, k_L, n and k_F, as function of the specific surface area, S_{BET}, for the CX-900 series.

Table 3 shows that the values of the Langmuir isotherm constant, k_L, of all activated carbon xerogels are up to 45 times greater than those of commercial carbons (BPL, NC35, R2030). The amount of adsorbate at monolayer coverage, q_{max}, of the non-activated carbon xerogel (CX), $q_{max} = 212$ mg g_C^{-1}, is increased after physical activation from 438 to 714 mg g_C^{-1} for CX-900-4 and CX-900-16, respectively. For comparison, the highest q_{max} observed for commercial carbons was in the case of sample R2030 (625 mg g_C^{-1}). For the physically activated carbon xerogels, the values of q_{max} (Fig. 3a) and k_L (Fig. 3b) increase together with the increase of S_{BET}.

As observed in the Langmuir model, the Freundlich constants, k_F and n, obtained for the non-activated carbon xerogel (CX) and for the activated samples (CX-900 series) are also higher than those of commercial carbons (Table 3). Activated carbon xerogels display k_F values ranging from 34 to 158 $mg_{MB}^{1-(1/n)}\, L^{1/n}\, g_C^{-1}$, and increase together with the specific surface area, S_{BET} (Fig. 3c). As a reference, the k_F values for BPL, NC35 and R2030 equal 3.46, 11.32 and 3.52 $mg_{MB}^{1-(1/n)}\, L^{1/n}\, g_C^{-1}$, respectively. The constant $1/n$ in the CX-900 series does not change with the activation treatment: $1/n$ remains in the 0.29–0.33 range

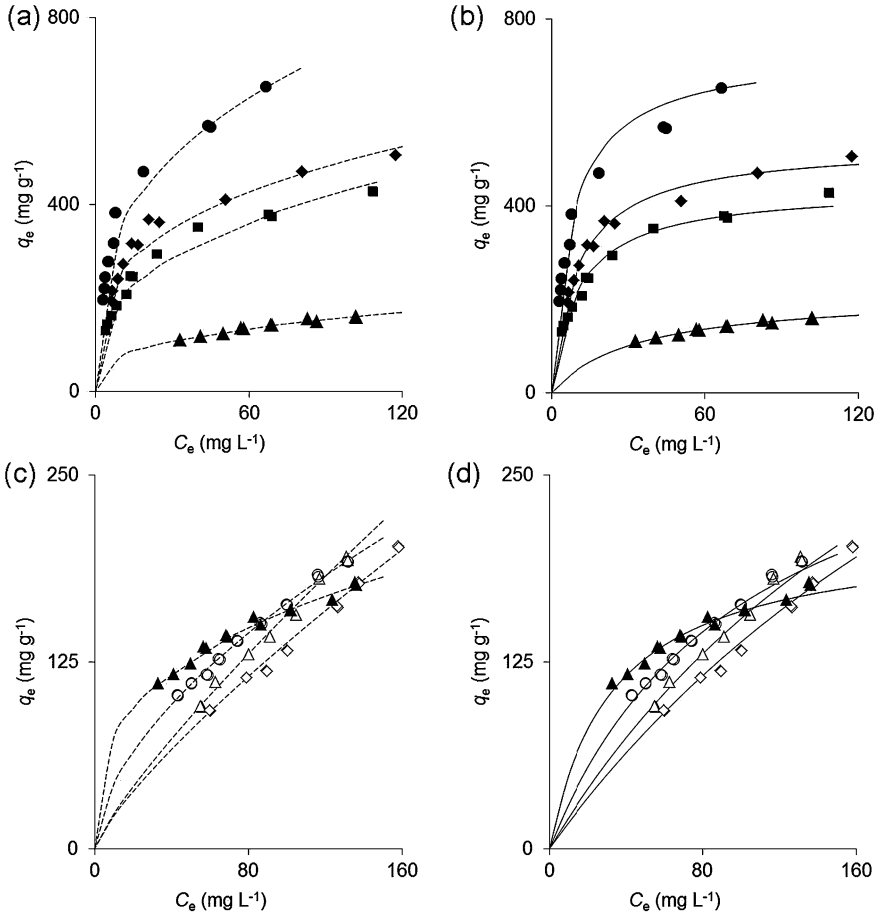

Fig. 2 Experimental MB-adsorption isotherms on the carbons and comparison with the Langmuir (- - -) and Freundlich isotherm (—) models. (**a**, **b**) Carbon xerogels CX (▲), CX-900-4 (■), CX-900-8 (♦), CX-900-16 (●); (**c**, **d**) Commercial carbons BPL (○), NC35 (△), and R2030 (◇). The non-activated carbon xerogel CX (▲) is reported as reference on the four figures

Table 3 Parameters of Langmuir and Freundlich isotherms

	Langmuir					Freundlich				ρ_{MB}
	q_{max} ($mg_{MB}\ g_C^{-1}$)	k_L ($L\ mg_{MB}^{-1}$)	R^2	P (%)	S_{MB}/S_{BET}	$1/n$	k_F ($mg_{MB}^{1-(1/n)}\ L^{1/n}\ g_C^{-1}$)	R^2	P (%)	($mmol_{MB}\ g_C^{-1}$)
CX	212.2	0.0298	0.9901	3.98	0.79	0.33	34.8	0.9884	2.30	0.66
CX-900-4	438.2	0.0930	0.9904	2.94	1.01	0.34	87.5	0.9889	4.01	1.37
CX-900-8	531.8	0.0955	0.9895	2.77	0.91	0.29	127.2	0.9859	3.15	1.66
CX-900-16	714.3	0.1270	0.9908	3.40	0.77	0.33	158.6	0.9826	5.13	2.23
BPL	555.2	0.0038	0.9829	4.38	1.58	0.83	3.4	0.9898	3.26	1.73
NC35	333.3	0.0096	0.9916	3.44	0.66	0.58	11.3	0.9953	1.72	1.04
R2030	625.1	0.0028	0.9828	2.84	1.58	0.80	3.5	0.9894	2.24	1.95

q_{max}: monolayer capacity of the adsorbent; k_L: Langmuir adsorption constant; $1/n$: Freundlich heterogeneity factor; k_F: Freundlich isotherm constant; R^2: correlation coefficient; P: normalized percentage of deviation; S_{MB}: surface area covered by methylene blue (MB); ρ_{MB}: density of MB-active sites

[a] g_C correspond to gram of carbon whereas mg_{MB} to milligram of MB

(Fig. 3d), whereas, the higher values of $1/n$ were observed for the commercial carbons in the 0.58–0.83 range.

3.4 Adsorption kinetics

To study the effect of the surface development on the MB-adsorption kinetics of carbon xerogels, three empirical models were applied: (i) the pseudo-first-order model; (ii) the pseudo-second-order model and (iii) the intraparticle diffusion model (Ip et al. 2010; Wang et al. 2010). The pseudo-first and pseudo-second order models describe the adsorption rate based on the adsorption capacity of the support. In accordance with Ho (2006), Ho and McKay (2000), the pseudo-first-order model can be written as:

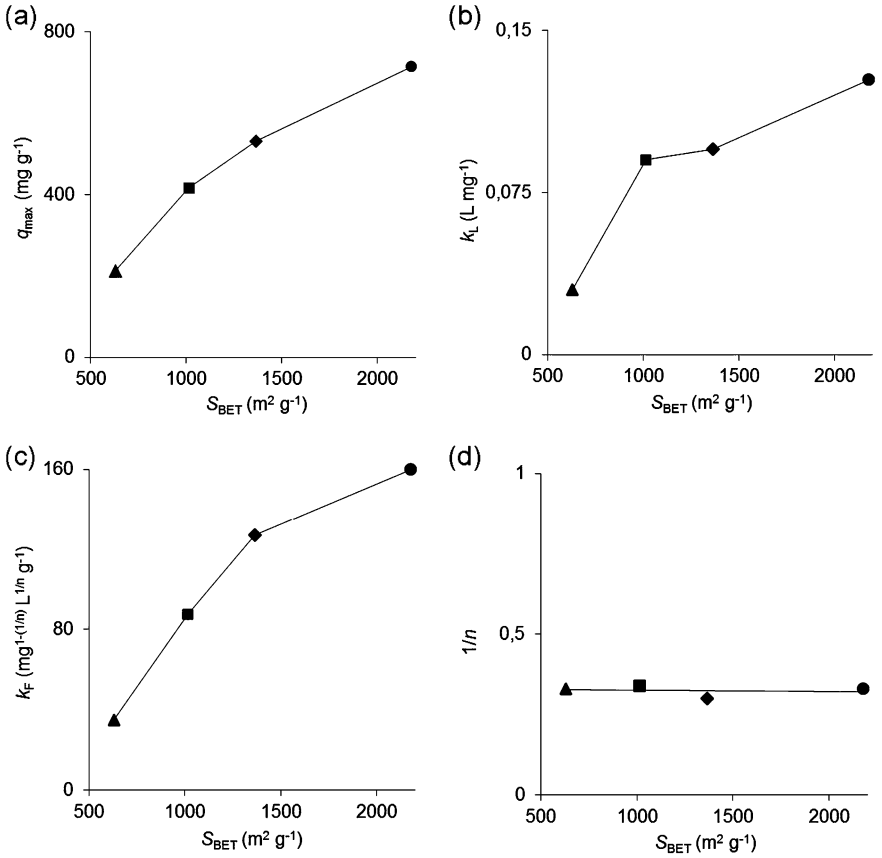

Fig. 3 Behavior of the Langmuir and Freundlich parameters: (**a**) q_{max}, (**b**) k_L, (**c**) k_F and (**d**) $1/n$ (**d**), as a function of the specific surface area (S_{BET}) for the carbon xerogel series: CX (▲), CX-900-4 (■), CX-900-8 (♦), CX-900-16 (●)

$$\frac{dq_t}{dt} = k_1(q_{eq} - q_t) \tag{7}$$

where q_{eq} (mol g_C^{-1}) and q_t (mol g_C^{-1}) are the adsorption capacities (or the amounts of MB-adsorbed) at equilibrium and at time $t\,(s)$, respectively and k_1 (s^{-1}) is the constant of the pseudo-first-order kinetic. Integration of Eq. (7), with the integration limits of $t = 0$ to $t = t$ and $q_t = 0$ to $q_t = q_t$, yields:

$$q_t = q_{eq}\left(1 - \exp(-k_1 t)\right) \tag{8}$$

which may be rearranged to a linear form (Ho 2006; Önal et al. 2007):

$$\ln(q_{eq} - q_t) = \ln q_{eq} - k_1 t \tag{9}$$

Thus, if experimental kinetic data correspond to a pseudo-first-order kinetic, then the plot of $\ln(q_{eq} - q_t)$ *vs.* t should be linear with a slope of k_1 and an intercept of $\ln q_{eq}$ on the $\ln(q_{eq} - q_t)$ axis.

Alternatively, Ho and McKay (2000) proposed that the driving force of the adsorption process is proportional to the available fraction of surface active sites. The kinetic equation rate can then be rewritten as Ho (2006), Ho and McKay (2000):

$$\frac{dq_t}{dt} = k_2(q_{eq} - q_t)^2 \tag{10}$$

After variable separation and integration ($t = 0$ to $t = t$ and $q_t = 0$ to $q_t = q_t$), Eq. (9) gives:

$$q_t = \frac{k_2 q_{eq}^2 t}{1 + k_2 q_{eq} t} \tag{11}$$

which may be rearranged to a linear form:

$$\frac{t}{q_t} = \frac{1}{h} + \frac{1}{q_{eq}} t \tag{12}$$

$$h = k_2 q_{eq}^2 \tag{13}$$

where k_2 is the rate constant of pseudo-second-order adsorption ($g_C\ mg_{MB}^{-1}\ min^{-1}$) and h is the initial adsorption rate ($mg_{MB}\ g_C^{-1}\ min^{-1}$). According to Eq. (12), if experimental kinetic data correspond to a pseudo-second-order kinetic, the graph of t/q_t against t should give a linear relationship, with an intercept of $1/h$ on the t/q_{eq} axis.

The correlation coefficients, R^2, for the linear plots of $\ln(q_{eq} - q_t)$ *vs.* t and t/q_t *vs.* t are displayed in Table 4. The linearized form of the pseudo-first-order model for all adsorbents shows R^2 values between 0.9660 and 0.9963, whereas the linearized form of the pseudo-second-order model displays R^2 values higher than 0.9930 for all adsorbents. From these results, one can conclude that the pseudo-second-order model provides the best correlation of the experimental data. Figure 4 compares the behavior of q_t as a function of time

Table 4 Kinetic parameters of pseudo-first-order and pseudo-second-order models

Sample	Pseudo-first-order			Pseudo-second-order		
	q_{eq} ($mg_{MB}\ g_C^{-1}$)[a]	k_1 (min^{-1})	R^2	q_{eq} ($mg_{MB}\ g_C^{-1}$)[a]	k_2 ($g_C\ mg_{MB}^{-1}\ min^{-1}$)[a]	R^2
CX	3.79	0.0045	0.9923	4.99	0.0007	0.9944
CX-900-4	3.48	0.0081	0.9660	4.07	0.0023	0.9954
CX-900-8	3.49	0.0122	0.9963	4.21	0.0028	0.9941
CX-900-16	3.61	0.0112	0.9914	4.34	0.0030	0.9935
BPL	3.25	0.0052	0.9926	3.92	0.0011	0.9924
NC35	3.06	0.0044	0.9959	4.40	0.0007	0.9968
R2030	3.04	0.0031	0.9721	3.79	0.0008	0.9956

q_{eq}: amount of MB adsorbed at equilibrium calculated from pseudo-first-order model or pseudo-second-order model; k_1: rate constant of the pseudo-first-order kinetic; k_2: rate constant of pseudo-second-order model

[a] g_C corresponds to gram of carbon whereas mg_{MB} to milligram of MB

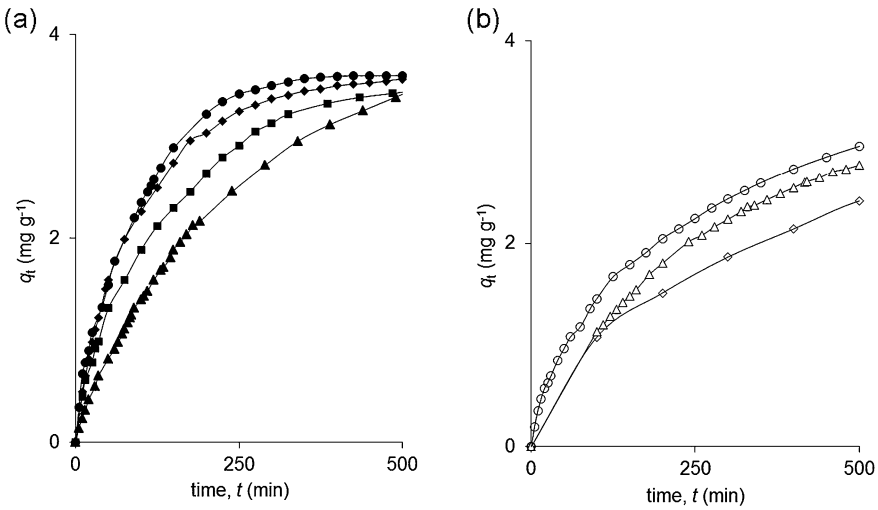

Fig. 4 Comparison of the experimental adsorption kinetic data: (**a**) carbon xerogels CX (▲), CX-900-4 (■), CX-900-8 (♦), CX-900-16 (●) and (**b**) commercial carbons: BPL (○), NC35 (△), R2030 (◊)

of the experimental data of the carbon xerogels (Fig. 4a) and of the commercial activated carbons (R2030, NC3, BPL, Fig. 4b). The parameters h and k_2 are displayed in Table 4. It can be observed that the values of the equation constant, k_2, are higher for the activated CXs than for the commercial carbons (Table 4): with k_2 values between 0.0023 and 0.0030 $g_C\ mg_{MB}{}^{-1}\ min^{-1}$ for activated CXs and from 0.0007 to 0.0011 $g_C\ mg_{MB}{}^{-1}\ min^{-1}$ for commercial carbons. Figure 5a displays the behavior of the initial adsorption rate, h, of CX-900 series as a function of specific surface area, S_{BET}. An increase of h is observed together with increase of S_{BET} or by effect of physical activation of CX.

Finally, considering that the pseudo-first- and pseudo-second-order models could not identify the diffusion mechanism (Wang et al. 2010), an intraparticle diffusion kinetic model was also applied. This model is expressed as (Wang et al. 2010; Kannan and Sundaram 2001; Wang and Li 2007):

$$q_t = k_{int(i)} t^{1/2} + c \tag{14}$$

where $k_{int(i)}$ is the intraparticle diffusion rate constant ($mg_{MB}\ g_C^{-1}\ min^{1/2}$) and c is the intercept on the q_t axis. According to Kannan and Sundaram (2001), the value of c gives an idea about the boundary layer thickness. The intraparticle diffusion model is proposed from the theory established by Weber and Morris (1962), which considers that the fractional approach to the equilibrium of solute adsorption can change as a function of $(Dt/r^2)^{1/2}$, where r is the particle radius and D is the diffusivity of solute within the particle (Wu et al. 2005). Thus, if the particle radius remains constant (25 μm $\leq r \leq$ 50 μm), then the fractional approach to equilibrium will change according to diffusion ability of solute within the carbon particle. In theory, the plot of q_t against $t^{1/2}$ is given by multiple linear ranges of different slope representing: (i) external surface adsorption or instantaneous adsorption stage (Wu et al. 2005) and (ii) intraparticle diffusion in pores of various separate size ranges (*e.g.* meso and micropores, typically) (Wang et al. 2010; Wang and Li 2007; Kumar et al. 2005). Figures 6a and 7

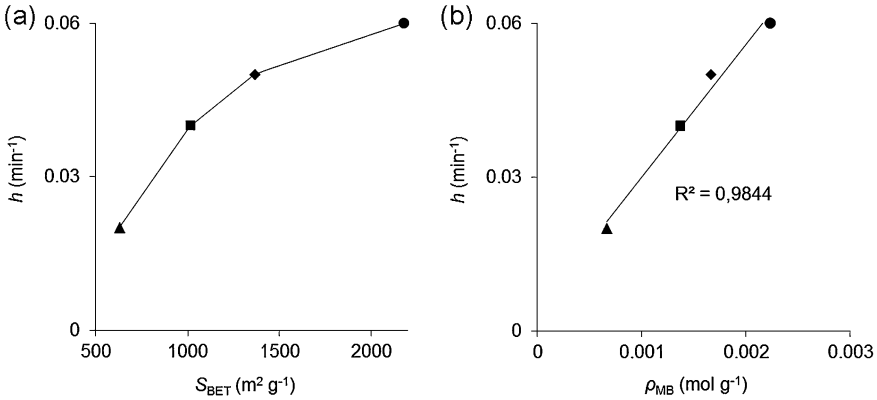

Fig. 5 Behavior of the initial adsorption rate h of the carbon xerogels (non-activated and activated) as a function of: (**a**) the specific surface area, S_{BET}, and (**b**) the density of MB-adsorption active sites, ρ_{MB}. CX (▲), CX-900-4 (■), CX-900-8 (♦), CX-900-16 (●)

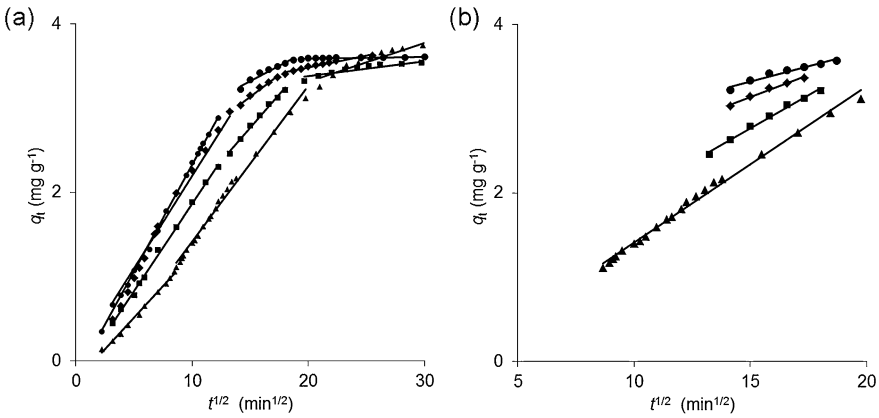

Fig. 6 (**a**) Root time plot for the adsorption of MB onto carbon: (**a**) carbon xerogels CX (▲), CX-900-4 (■), CX-900-8 (♦), CX-900-16 (●) and (**b**) root time plot for the adsorption of MB but in the 7–20 $min^{1/2}$ range

display these plots for adsorption of MB onto CX, CX-900 series (Fig. 6a) and onto commercial carbons (Fig. 7). In all cases, three consecutive linear stages are observed. In accordance with Wang et al. (2010), the first linear portion of the curve corresponds to a process governed by external surface adsorption; the second linear portion can be assigned to the gradual adsorption step where intraparticle diffusion is the rate-limiting phenomenon; the third portion is the final equilibrium stage where the MB concentration gradient between the liquid outside the carbon grains and the solution trapped in the carbon pores tends to zero.

Table 5 displays the intraparticle diffusion rate constants ($k_{int(i)}$) of each linear stage for all the carbons, with i corresponding to the stage number. It can be observed that the values of $k_{int(1)}$ are higher for the CX-900-series than for the non-activated xerogel carbon (CX) and for the commercial carbons. In addition, an increase of $k_{int(1)}$ is observed together with the augmentation of activation time (t_{act}), *i.e.* from 0.20 $mg_{MB}\, g_C^{-1}\, min^{-1/2}$ for CX-900-4 to 0.25 $mg_{MB}\, g_C^{-1}\, min^{-1/2}$ for CX-900-16. Nevertheless, an opposite behavior of the diffusion rate constants of the second linear stage, $k_{int(2)}$, is observed; a decrease of $k_{int(2)}$ is determined together with the augmentation of activation time (t_{act}), *i.e.* from 0.16 $mg_{MB}\, g_C^{-1}\, min^{-1/2}$ for CX-900-4 to 0.06 $mg_{MB}\, g_C^{-1}\, min^{-1/2}$ for CX-900-16. Figure 6b compares in detail, the second linear portion corresponding to

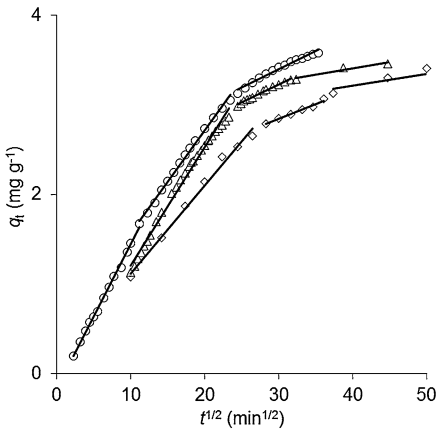

Fig. 7 Root time plot for the adsorption of MB onto commercial carbons: BPL (○), NC35 (△), R2030 (◇)

CX-series, from 10 to 20 $min^{1/2}$. Besides the decrease of $k_{int(2)}$ together with the increase of activation time (t_{act}), two additional phenomena are observed: (i) for the non-activated carbon, CX, the stage of intraparticle diffusion control is started at 75 min ($t^{1/2} = 8.66\ min^{1/2}$) and is completed after 315 min (at 390 min, $t^{1/2} = 19.74\ min^{1/2}$), whereas for CX-900-series this stage is started at 175 min and lasts only nearly 175 min (up to $t^{1/2} = 18.70\ min^{1/2}$); (ii) the values of intercept, c, of the CX-900-series increase with the increase

Table 5 Kinetic parameters of intraparticle diffusion model

Sample	Intraparticle diffusion rate constant, $k_{int(i)}$ [a]		
	$k_{int(1)}$ ($mg_{MB}\ g_C^{-1}\ min^{1/2}$)	$k_{int(2)}$ ($mg_{MB}\ g_C^{-1}\ min^{1/2}$)	$k_{int(3)}$ ($mg_{MB}\ g_C^{-1}\ min^{1/2}$)
CX	0.15	0.18	0.046
CX-900-4	0.20	0.15	0.017
CX-900-8	0.24	0.10	0.027
CX-900-16	0.25	0.06	0.001
BPL	0.16	0.11	0.040
NC35	0.13	0.04	0.013
R2030	0.02	0.03	0.013

$k_{int(i)}$: is the diffusion rate constant (i corresponds to the linear portion number)

[a] g_C corresponds to gram of carbon whereas mg_{MB} to milligram of MB

of activation time, and are significantly larger than that of CX. These results show that, while the diffusion mechanism is better represented by the intraparticle diffusion step within CX particles, the diffusion of MB within CX-900-series is only limited by the intraparticle diffusion control during the final MB-adsorption equilibrium step.

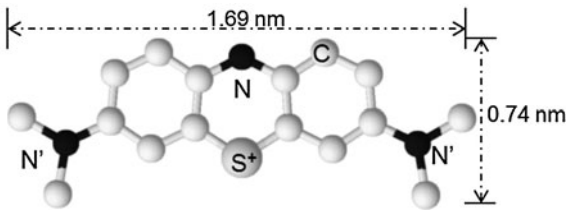

Fig. 8 Molecular structure of Methylene Blue, MB

4 Discussion

4.1 Textural properties and surface chemistry characterization

As shown by Contreras et al. (2010), the physical activation of carbon xerogels (CXs) using carbon dioxide allows the production of materials with a well-developed microporosity without any alteration of the mesopores formed during the gel synthesis. The development of micropores can be interpreted in terms of increase of specific surface area, S_{BET}. As shown in Fig. 1a, for the CX-900-series, S_{BET} increases quite linearly with the increase of activation time, reaching S_{BET} values of 2180 $m^2\ g_C^{-1}$ for CX-900-16. In addition, the increase of specific surface area is accompanied by a chemical clearing of carbon xerogel surface. In the CX-900 series the amount of CO (or CO_2) desorbed by surface area unit, $n_{A,CO}$ and n_{A,CO_2}, decreases with the increase of S_{BET} (Fig. 1b), reflecting an important diminution in the amounts of oxygen surface groups detected by surface area unit. Therefore, even if the gel synthesis allows of production of a CX superficially clean, with low $n_{A,CO}$ and n_{A,CO_2} values (compared with commercial carbons, Table 2), a decrease in the oxygen-containing surface groups by surface area unit is observed during physical activation of CX and with the increase of t_{act}.

4.2 Adsorption equilibrium isotherms

The modifications observed in the chemical and physical properties of carbon xerogels after physical activation using CO_2 affect the adsorption process. The effect of activation treatment with CO_2 on the MB adsorption capacity of carbon xerogels is studied in Figs. 2a–2b. All adsorption isotherms show L-shaped curves according to the classification of Giles et al. (1960, 1974). The initial slope or form of these curves shows that the surface site availability decreases with increasing the amount of adsorbed MB. Thus, when the majority of surface sites are filled, it becomes increasingly difficult for a molecule of dye to find a vacant site. In accordance with Giles et al. (1960), this behavior implies either that the adsorbed molecules are not vertically oriented or that there is no strong competition between the solvent and the adsorbate to occupy the active surface sites. This could mean that within the interactions between carbons active surface sites and the adsorbate, the contact of the aromatic entity of MB and the active sites plays an important role (Fig. 8). The activation degree of these surface sites and the molecular orientation of MB adsorbed on the carbon surface can be defined by: (i) the type and amount of oxygen-containing surface groups on the carbon, (ii) the π-electron density on the graphene layers and (iii) the physicochemical properties of the adsorbate, MB (Moreno-Castilla 2004).

The structure of the MB cation is shown in Fig. 8 (Hahner et al. 1996). The MB is a heteroaromatic molecule that contains one sulfur and one nitrogen atom in the aromatic moiety. The aromatic unit is planar and has two dimethylamino groups attached. The whole molecule is conjugated and the π-orbitals are delocalized over the entire molecule (except for the methyl groups) (Hahner et al. 1996). The positive charge is best stabilized by the amino group (N) and the S atom (Fig. 8). Hence, the maximal electrostatic interaction is expected when the longest edge of these atoms

is in contact with surface sites charged negatively and/or with functional surface groups of high electronic density, such as oxygen-containing surface groups. Nevertheless, several studies (Moreno-Castilla 2004) have demonstrated that, while electrostatic interactions are important, π–π dispersion interactions appear to be dominant in the adsorption of aromatic solutes. These π–π interactions can appear as a consequence of donor/acceptor interaction between the π-electron density of the graphene layers on carbon surface and delocalized π-orbitals of the MB molecule. Therefore, a flat orientation of the MB molecules in contact with carbon surface is assumed, the longitudinal axis of the adsorbed molecules being parallel to the adsorbent surface (Hahner et al. 1996).

Figure 2 shows that the experimental data of adsorption isotherms fit well with both the Langmuir model and the Freundlich model.

First, the Langmuir isotherm model (Eq. (2)) suggests that adsorption takes place on specific homogeneous surface active sites to saturated monolayer coverage of dye molecules, q_{max}, and that the binding energy of this adsorption is related to the Langmuir isotherm constant, k_L (Yu et al. 2009; Allen et al. 2004). Figure 3a shows that the capacity of adsorption at monolayer coverage, q_{max}, of the carbon xerogel series (CX and activated samples CX-900) is increased by effect of the increase of specific surface area. If one assumes that MB molecules are adsorbed in flat orientation and considering that its effective area is 7.2×10^5 m^2 by mol of MB ($m^2\ mol_{MB}^{-1}$, Hahner et al. 1996), then the specific surface area covered by MB at monolayer coverage, S_{MB}, can be calculated by multiplying q_{max} (expressed in $mol_{MB}\ g_C^{-1}$) by $7.2 \times 10^5\ m^2\ mol_{MB}^{-1}$. From Table 3, it is observed that the ratio between the specific surface area covered by MB, S_{MB}, and S_{BET} (S_{MB}/S_{BET}) decreases from 1.01 for CX-900-4 to 0.77 for CX-900-16. This means that the formation of dye monolayer is carried out without aggregation ($S_{MB}/S_{BET} \leq 1$) and that the intermolecular space between flat-oriented MB-molecules increases with the specific surface area, S_{BET}.

The increase of the intramolecular space means a decrease in the intermolecular interactions, allowing a greater dispersion of π–π interactions between the adsorbate and the graphene layers, and leading to an increase in the binding energy of MB-adsorption. In fact, Fig. 3b shows that the k_L values for the CX-900 series increase with S_{BET}, as a consequence of physical activation and, possibly, as a result of the increase in binding energy of MB-adsorption. The π–π interactions between the π-electron density of the graphene layers on carbons surface and delocalized π-orbitals of MB, can be the result of the chemical reactions occurring at the solid/liquid interface leading to the formation of a MB-CX adsorptive structure, similar to the one observed by Yan et al. in the adsorption of MB onto carbon nanotubes (Yan et al. 2005). Therefore, for the MB-adsorption, the active surface sites are the π-aromatic electrons of the graphene layers (Moreno-Castilla 2004). Consequently, the significance of these aromatic electrons or the amount of surface active sites per gram of carbon xerogel (labeled MB-active sites density, ρ_{MB}) increases when the amount of oxygen surface groups decreases. The density of MB-active sites, ρ_{MB}, corresponds to the value of q_{max} but expressed in $mol_{MB}\ g_C^{-1}$.

Finally, the physical activation with CO_2 leads to the improvement in the MB adsorption ability of carbon xerogels, reaching k_L values up to 13, 30 and 45 times higher than in the case of commercial carbons NC35, BPL, and R2030, respectively (Table 3). In addition, the capacity of MB-adsorption at monolayer coverage, q_{max}, of the activated carbon CX-900-16 ($\cong 714\ mg_{MB}\ g_C^{-1}$) not only was superior to those shown by reference commercial carbons (NC35, BPL, R2030), but was also comparable or higher than those reported by literature for different activated carbons (Girgis et al. 2011; Benadjemia et al. 2011; Zhou et al. 2011).

Second, the Freundlich isotherm model is another approach for adsorption on an amorphous or heterogeneous surface (Wong et al. 2003). The Freundlich equation (3) is an empirical model used to describe heterogeneous systems, where $1/n$ corresponds to the heterogeneity factor of adsorbent and k_F, the Freundlich constant, represents the adsorption capacity of the adsorbent (Wang et al. 2010). Like in the case of the Langmuir isotherm model, the physical activation of CX causes a significantly increase in k_F together with the increase of S_{BET}, as detailed in Fig. 3b. The MB adsorption capacity of all synthesized carbon xerogels, k_F, is superior to those displayed by the commercial carbons NC35, BPL and R2030 (Table 3). Nevertheless, the factor $1/n$ of the non-activated sample (0.32) is smaller than those corresponding to commercial carbons, between 0.58 and 0.83. This means that, compared to the commercial carbons studied, the non-activated carbon xerogel (CX) is a material with a higher homogeneity of surface active sites. In addition, Fig. 3d shows the behavior of this factor, $1/n$, of CX-900-series as a function of specific surface area, S_{BET}. It is observed that the $1/n$ values remains in the 0.29–0.33 range, whereas S_{BET} increase. So, for the CX-900-series the homogeneity of the surface does not change as an effect of physical activation with CO_2 (Fig. 3d).

4.3 Adsorption kinetics

In order to obtain information about the adsorption mechanisms, a study of adsorption kinetics of methylene blue was realized applying three kinetic models: the pseudo-first-order model, the pseudo-second-order model and the intraparticle diffusion model. Table 4 shows that the experimental kinetic data of all carbons are well represented by

the pseudo-second-order kinetic model (R^2 values). This means that the kinetic order is two with respect to the number of available active sites ($q_{eq} - q_t$) for MB adsorption, see Eq. (11). Therefore, the rate expression is not described by the adsorption capacity of the carbon xerogels only: other phenomena can be considered, such as chemical bonding or π–π interactions between the adsorbate and the carbon graphene layers (Moreno-Castilla 2004; Yan et al. 2005). These reactions could be represented in two ways (Eqs. (15a)–(15b) and (16)):

$$\text{XC-CO}^- + \text{MB}^+ \rightarrow \text{XC-CO-MB} \tag{15a}$$

$$\text{XC-COO}^- + \text{MB}^+ \rightarrow \text{XC-COO-MB} \tag{15b}$$

$$\text{XC-Ar}_{\pi e} + \text{MB}_{\pi e} \rightarrow \text{XC-Ar}_{\pi e-\pi e}\text{MB}(\pi\text{–}\pi \text{ interactions}) \tag{16}$$

The first way (Eqs. (15a) and (15b)) considers that the carbon surface contains polar functional groups (–CO^-, –COO^-) which participate in the chemical bonding, allowing cationic dye adsorption (MB^+). Nevertheless, from the chemical characterization of the synthesized carbons, it was observed that, during their physical activation and with the increase of t_{act}, a decrease in the oxygen-containing surface groups by surface area unit is observed. In addition, it is also observed that under our MB-absorption kinetics conditions, at a constant pH of 6.5 (pH < PZC, Table 2), the carbon surface is positively charged, producing a repulsion of the cationic dye (MB^+). In both cases, the carbon surface charges and the physical activation would cause a diminution in the initial adsorption rate of MB, h, obtained from pseudo-second-order model (Eq. (14)). However, from Fig. 5a one observes that h increases together with the specific surface area, S_{BET}, in the CX-900 series.

In the second way, as it was proposed in the MB adsorption equilibrium isotherms studies, the π-aromatic electrons of the carbon graphene layers (XC-$Ar_{\pi e}$) are considered as the active surface sites and the density of these MB-active sites, ρ_{MB}, was determined. Thus, π–π interactions between MB ($MB_{\pi e}$) and the graphene layers would favor the MB adsorption (XC-$Ar_{\pi e-\pi e}$MB, Eq. (16)). The behavior of the initial adsorption rate, h, as a function of ρ_{MB} for CX-900 series is displayed in Fig. 5b. One observes that the initial adsorption rate, h, increases when the density of MB active sites, ρ_M, increases, possibly because the MB adsorption mechanism is governed by π–π interactions.

Several works propose that the adsorption of dye molecules can take place in pore diameters of 1.3–1.8 times the dye molecular width (Ip et al. 2010; Li et al. 2002). In accordance with Giles et al. (1960, 1974), most of dye molecules probably diffuse into the pore structure through longitudinal position. This diffusion is a random process and it is restricted by the shortest side of dye molecule (Ip et al. 2010). Different estimations of the MB-molecule dimensions (Hahner et al. 1996) suggest that the average value of the length is 1.69 nm, 0.74 nm for the width and 0.38 nm for the thickness (Fig. 8). Therefore, if one assumes that the MB-molecule diffuses into the pores through longitudinal position by the shortest side (0.74 nm), then MB-adsorption could take place into pore with diameters larger or equal to $1.3 \times 0.74 = 0.96$ nm. On the contrary, the MB-diffusion into the pore structure would be hindered in pore diameters smaller that 0.96 nm. On the one hand, the microporous structure developed by the carbon xerogel (CX) before physical activation displays an average microporore size values (L) smaller that 0.96 nm, $L = 0.79$ nm (see Table 2 in Contreras et al. 2010). In this case, the probability of MB-diffusion into the micropore structure is low, limiting the MB-adsorption rate by effect of intraparticle diffusion. On the other hand, after physical activation at 900 °C (CX-900-series), L values between 0.96 and 1.40 nm are reached (Table 2 in Contreras et al. 2010). This means that the probability of MB-diffusion into the micropore increases, which decreases the effect of MB-adsorption rate limitation *via* intraparticle diffusion processes. Consequently, the possibility of interaction between MB-molecules and active sites inside the micropores increases, enhancing the MB-adsorption rate *via* adsorption reactions occurring at a solid/liquid interface. In fact, the analysis of the adsorption kinetics shows an enhancement of the MB-adsorption rate together with the microporosity development in the carbon xerogels activated at 900 °C.

5 Conclusions

The effect of CO_2 activation of a carbon xerogel at 900 °C on the textural and chemical properties resulted in several changes in the MB-absorption performances of the final carbon material. First, according to the Langmuir isotherm analysis, the development of the specific surface area, S_{BET}, and the cleaning of surface graphene layers both led to significant enhancement in the MB-absorption capacity (up to 2180 $m^2\,g_C^{-1}$) together with an increase in the adsorption binding energy, k_L. This energy can be attributed to an increase of the π–π dispersion interactions between the MB molecules and the graphene layers (Eqs. (15a) and (15b)). Second, in agreement with the Freundlich isotherm analysis, an increase in the carbon surface homogeneity was produced, due to the diminution in the amount of oxygen surface groups by surface area unity after activation at 900 °C. This implies the formation of equivalent sites potentially actives for the MB-adsorption. Third, related to MB-adsorption kinetics analysis, it was found that two different mechanisms control the MB-adsorption rate of the synthesized carbon xerogels.

Regarding the micropore structure, the average micropore diameter of the non-activated carbon xerogel (CX, with $L = 0.74$ nm) can originate a restriction in the diffusion of MB into the micropore structure, limiting the MB-adsorption rate by effect of intraparticle diffusion mechanism. The physical activation at 900 °C (CX-900-series) leads to the development of microporosity with a wider size range, diminishing the restriction by intraparticle diffusion and hence, enhancing the MB-adsorption rate *via* mechanism of adsorption by reactions occurring at solid/liquid interface.

Finally, the capacity of MB-adsorption at monolayer coverage, q_{max}, of the activated carbon CX-900-16 ($\cong 714\ mg_{MB}\ g_C^{-1}$) was higher than those shown by reference commercial carbons (NC35, BPL, R2030), and was even higher than those reported in the literature for different activated carbons (Rafatullah et al. 2010). The activation with CO_2 of carbon xerogels obtained by pyrolysis of resorcinol-formaldehyde aqueous gels produces materials with excellent MB-adsorption capacities form aqueous solutions that can be used with high efficiency in water decontamination processes.

Acknowledgements C.P. is postdoctoral researcher of the F.R.S.-FNRS (Belgium). The Belgian authors thank the Fonds de Recherche Fondamentale Collective, the Ministère de la Region Wallonne and the Interuniversity Attraction Pole (IAP-P6/17) for their financial support.

References

Allen, S.J., McKay, G., Porter, J.F.: J. Colloid Interface Sci. **280**, 322–333 (2004)
Benadjemia, M., Millière, L., Reinert, L., Benderdouche, N., Duclaux, L.: Fuel Process. Technol. **92**, 1203–1212 (2011)
Contreras, M.S., Páez, C.A., Zubizarreta, L., Léonard, A., Blacher, S., Olivera-Fuentes, C.G., Arenillas, A., Pirard, J.-P., Job, N.: Carbon **48**, 3157–3168 (2010)
El Qada, E.N., Allen, S.J., Walker, G.M.: Chem. Eng. J. **135**, 174–184 (2008)
Elisangela, F., Andrea, Z., Fabio, D.G., de Menezes Cristiano, R., Regina, D.L., Artur, C.-P.: Int. Biodeterior. Biodegrad. **63**, 280–288 (2009)
Figueiredo, J.L., Pereira, M.F.R., Freitas, M.M.A., Órfão, J.J.M.: Carbon **37**, 1379–1389 (1999)
Freundlich, H.: Z. Phys. Chem. **57**, 86 (1906)
Giles, C.H., MacEwan, T.H., Nakhwa, S.N., Smith, D.: Journal of the Chemical Society (Resumed) (1960) 3973–3993
Giles, C.H., D'Silva, A.P., Easton, I.A.: J. Colloid Interface Sci. **47**, 766–778 (1974)
Girgis, B.S., Attia, A.A., Fathy, N.A.: Desalination **265**, 169–176 (2011)
Gommes, C.J., Job, N., Pirard, J.-P., Blacher, S., Goderis, B.: J. Appl. Crystallogr. **41**, 663–668 (2008)
Granados-O., G., Páez-M., C.A., Martínez-O., F., Páez-Mozo, E.A.: Catal. Today **107–108**, 589–594 (2005)
Hahner, G., Marti, A., Spencer, N.D., Caseri, W.R.: J. Chem. Phys. **104**, 7749–7757 (1996)
Hamdaoui, O.: J. Hazard. Mater. **135**, 264–273 (2006)
Ho, Y.-S.: J. Hazard. Mater. **136**, 681–689 (2006)
Ho, Y.S., McKay, G.: Water Res. **34**, 735–742 (2000)
Ip, A.W.M., Barford, J.P., McKay, G.: Chem. Eng. J. **157**, 434–442 (2010)
Jin, X.-C., Liu, G.-Q., Xu, Z.-H., Tao, W.-Y.: Appl. Microbiol. Biotechnol. **74**, 239–243 (2007)
Job, N., Heinrichs, B., Lambert, S., Pirard, J.-P., Colomer, J.-F., Vertruyen, B., Marien, J.: AIChE J. **52**, 2663–2676 (2006)
Job, N., Pirard, R., Marien, J., Pirard, J.-P.: Carbon **42**, 619–628 (2004)
Kannan, N., Sundaram, M.M.: Dyes Pigm. **51**, 25–40 (2001)
Karaca, S., Gürses, A., AçIkyIldIz, M., Ejder, M.: Microporous Mesoporous Mater. **115**, 376–382 (2008)
Kumar, K.V., Ramamurthi, V., Sivanesan, S.: J. Colloid Interface Sci. **284**, 14–21 (2005)
Labanda, J., Sabaté, J., Llorens, J.: Chem. Eng. J. **166**, 536–543 (2011)
Lambert, S., Job, N., D'Souza, L., Pereira, M.F.R., Pirard, R., Heinrichs, B., Figueiredo, J.L., Pirard, J.-P., Regalbuto, J.R.: J. Catal. **261**, 23–33 (2009)
Langmuir, I.: J. Am. Chem. Soc. **40**, 1361–1403 (1918)
Li, L., Quinlivan, P.A., Knappe, D.R.U.: Carbon **40**, 2085–2100 (2002)
Misra, D.N.: Surf. Sci. **18**, 367–372 (1969)
Moreno-Castilla, C.: Carbon **42**, 83–94 (2004)
Nacèra, Y., Aicha, B.: Chem. Eng. J. **119**, 121–125 (2006)
Nataraj, S.K., Hosamani, K.M., Aminabhavi, T.M.: Desalination **249**, 12–17 (2009)
Önal, Y., Akmil-Basar, C., SarIcI-Özdemir, Ç.: J. Hazard. Mater. **146**, 194–203 (2007)
Páez, C.A., Poelman, D., Pirard, J.-P., Heinrichs, B.: Appl. Catal. B, Environ. **94**, 263–271 (2010)
Potgieter, J.H.: J. Chem. Educ. **68**, 349 (1991)
Rafatullah, M., Sulaiman, O., Hashim, R., Ahmad, A.: J. Hazard. Mater. **177**, 70–80 (2010)
Raposo, F., De La Rubia, M.A., Borja, R.: J. Hazard. Mater. **165**, 291–299 (2009)
Regalbuto, J.: In: Regalbuto, J. (ed.) Catalyst Preparation: Science and Engineering, pp. 297–318. CRC Press, Taylor & Francis Group, Boca Raton (2007)
Stavropoulos, G.G., Zabaniotou, A.A.: Microporous Mesoporous Mater. **82**, 79–85 (2005)
Stephenson, R.J., Duff, S.J.B.: Water Res. **30**, 781–792 (1996)
Szygula, A., Guibal, E., Palacín, M.A., Ruiz, M., Sastre, A.M.: J. Environ. Manag. **90**, 2979–2986 (2009)
Tan, I.A.W., Ahmad, A.L., Hameed, B.H.: J. Hazard. Mater. **154**, 337–346 (2008)
Wang, S., Li, H.: Dyes Pigm. **72**, 308–314 (2007)
Wang, L., Zhang, J., Zhao, R., Li, C., Li, Y., Zhang, C.: Desalination **254**, 68–74 (2010)
Weber, W.J., Morris, J.C.: Advances in Water Pollution Research: Removal of Biologically Resistant Pollutants from Waste Water by Adsorption. Pergamon, Oxford (1962)
Wong, Y.C., Szeto, Y.S., Cheung, W.H., McKay, G.: Langmuir **19**, 7888–7894 (2003)
Wu, F.-C., Tseng, R.-L., Juang, R.-S.: J. Colloid Interface Sci. **283**, 49–56 (2005)
Yamashita, J., Shioya, M., Kikutani, T., Hashimoto, T.: Carbon **39**, 207–214 (2001)
Yan, Y., Zhang, M., Gong, K., Su, L., Guo, Z., Mao, L.: Chem. Mater. **17**, 3457–3463 (2005)
Yu, J.-X., Li, B.-H., Sun, X.-M., Yuan, J., Chi, R.-a.: J. Hazard. Mater. **168**, 1147–1154 (2009)
Zhou, G., Tian, H., Sun, H., Wang, S., Buckley, C.E.: Chem. Eng. J. **171**, 1399–1405 (2011)
Zubizarreta, L., Arenillas, A., Pirard, J.-P., Pis, J.J., Job, N.: Microporous Mesoporous Mater. **115**, 480–490 (2008)
Zubizarreta, L., Arenillas, A., Pis, J., Pirard, J.-P., Job, N.: J. Mater. Sci. **44**, 6583–6590 (2009)